ISSN 0010-9525, Cosmic Research, 2017, Vol. 55, No. 4, pp. 235–247. © Pleiades Publishing, Ltd., 2017.
Original Russian Text © T.K. Breus, A.M. Krymskii, 2017, published in Kosmicheskie Issledovaniya, 2017, Vol. 55, No. 4, pp. 249–262.

Remnant Magnetic Fields of Mars and Their Interaction with the Solar Wind

T. K. Breus[a], * and A. M. Krymskii[b], **

[a]*Space Research Institute, Russian Academy of Sciences, Moscow 117997, Russia*
[b]*Southern Federal University, Rostov-on-Don 344008, Russia*
**e-mail: breus36@mail.ru*
***e-mail: amkrym@yahoo.com*

Received March 10, 2016

Abstract—This work presents a review of studies of the Martian magnetic fields during the early Soviet missions to Mars in 1971–1974, which never approached Mars by closer than 1000 km before the experiment with the Magnetometer/Electronic Reflectometer (MAG/ER) on board the *Mars Global Surveyor* spacecraft, which could descend to altitudes of 80–100 km. At present, the experiment with the magnetometer (MAG) onboard the American *MAVEN* spacecraft adds new data, but the map of distribution of remnant magnetic fields of Mars and the picture of their interaction with the solar wind are already formed and, at its core, obviously, will not be revised. Thus, it would be very instructive to consider the following in detail: (a) what is already known regarding the features and distribution of remnant magnetic fields on Mars; (b) how they control the interaction of solar wind with a weakly magnetized planet (Mars); and (c) what is its distinction from another nonmagnetized planet (Venus).

DOI: 10.1134/S0010952517040025

INTRODUCTION

Studies of the intrinsic magnetic field of Mars began together with the missions to other planets. The characteristics of the intrinsic magnetic field of Mars could be a critical point in understanding the planetary dynamo processes being sensitive to the evolution of the crust, mantle and core of terrestrial-group planets. Today, the overall distribution of the magnetic fields and their influence on the properties of Martian atmosphere and ionosphere and the features of their interaction with the solar wind have been settled. However, some issues, such as (a) the formation and properties of boundaries in the region of solar wind flowing around the planet and the remnant magnetic fields effect on its shape; (b) the properties of mini-magnetospheres formed by remnant magnetic fields; and (c) the origin of the Martian magnetotail, which exceeds exceeding the Venusian magnetotail in dimensions, etc., remain disputed.

At the end of 2015, the first publications on the results of the *MAVEN* mission to Mars began to appear. The *MAVEN* spacecraft is designed to study the magnetic fields and plasma at altitudes of 120 km (during periods of deep immersion) and higher. In the experiment with a magnetometer on the *MAVEN* spacecraft, special attention is paid to the high accuracy of measurements and to reducing the influence of the magnetic field of the spacecraft itself [1]. The data on magnetic fields will be used to determine the role of plasma oscillations, reconnection, and the bulk plasma properties in the atmospheric loss processes and, in general, in the dynamics of interaction with the solar wind [1]. The *MAVEN* spacecraft, which revolves over the polar orbit around Mars, is expected to operate for more than two Martian years.

The overview of the results of previous missions to Mars, which concerns the planetary magnetic field and its role in the interaction with the solar wind flow, will allow one to identify the tasks on which the following actions can be focused: (a) subsequent comparative analysis of the results of *MAVEN* and other missions and (b) studying the long-term (over the scales of solar activity cycle) variability of Mars' interactions with the solar wind flow.

For this reason, it is of interest to accumulate and analyze all available data on the magnetic fields of Mars obtained in previous missions to the planet once again, and to try to answer the remaining questions. This is the subject of this review.

1. RESULTS OF EARLY MISSIONS

Initial measurements of the magnetic field of Mars have been carried out on the *Mars-2, -3* and *-5* SC in 1971–1974 [2, 3]. Simultaneous measurements of plasma properties and magnetic fields, which allowed the characteristic features in the solar wind (SW)

interaction with Mars to be established, were presented in papers [4–6]. These studies have revealed some similarity with the pattern of SW interaction with the terrestrial magnetosphere. In particular, according to the data of [7], a drastic change in the direction of the measured magnetic field was observed in the region of closest approach of the satellites to Mars: approximately at the altitude of 1100 km (on January 1, 1972, *Mars-2*, or on January 21, 1972, *Mars-3*). Upon approaching the planet, the magnitude of the magnetic field increased to 30 nT. The plasma measurement data have shown that, simultaneously with this phenomenon, a drop in the integral electron fluxes could be observed in this region [5], along with the deceleration of the ion flow [6]. The viewpoints on the nature of changes in the plasma and magnetic field characteristics close to Mars have differed.

The authors of [4, 7] concluded that the spacecraft have crossed the boundary of the intrinsic magnetosphere of Mars because the similar behavior of plasma and magnetic fields was typical of the Earth's magnetosphere (see, e.g., [8]). The authors of [9] explained the magnetic data exclusively by the interplanetary magnetic field (IMF) drapped around the planetary obstacle without addressing the intrinsic magnetic field of Mars. Johnston and Axford; in an unpublished report, they suggested that a weak intrinsic magnetic field of Mars might be confined within a lower ionosphere [10]. Thus, the nature of the Martian magnetic field could not be specified using the data obtained on spacecraft that did not approach Mars closer than approximately 1000 km.

According to the data obtained on the *Viking-1* and *Viking-2* landers in 1976, the maximum pressure of plasma of the Martian ionosphere is not sufficient to balance the median dynamic pressure of the SW [11]. Based on this fact, the authors of [11] concluded that the Martian ionosphere, but it was impossible to specify their nature.

The authors of [12] noted that the Martian atmosphere in the altitude range of 450–500 km possesses a high concentration of heavy components (oxygen) and light components (hydrogen), and this concentration exceeds that of heavy components in the atmosphere of Venus (because of lower gravitational attraction). In the charge exchange of SW protons with a hydrogen corona, the effective mass of a plasma ion does not change, but the momentum and energy flow in plasma decreases. However, in the case of the charge exchange of SW protons with a hot oxygen corona, the plasma ion mass increases by 15 atomic mass units (a.m.u.), which results in decelerating the flow. Because the IMF is weak near Mars, the Larmor radius of the O^+ ion is comparable to the radius of Mars [13]. Thus, the O^+ ions are only weakly coupled with the IMF and incompletely picked-up by the plasma flow. As a consequence, the effect of mass loading is weakened. At the same time, in the transition region near Venus the turbulence is enhanced [14]. With accounting for the observational data on the turbulence level, it was shown that the turbulence significantly increases the efficiency of picking up O^+ ions near Mars.

Thus, the results of early planetary missions indicated that, because of weakness of the intrinsic magnetic field of Mars, the solar wind interaction with this planet is much more complicated than the interactions with the other terrestrial-type planets of group, including Earth and Venus.

2. RESULTS OF STUDYING THE MAGNETIC FIELD OF MARS ON PHOBOS-2 SPACECRAFT AND AMERICAN *MARS GLOBAL SURVEYOR* SPACECRAFT

In 1989, before transferring the *Phobos-2* spacecraft into the circular orbit, the plasma and magnetic measurements in the closest vicinity to Mars have been carried out on four elliptical orbits with the pericenter altitude of ~850 km, which is slightly closer to the planet than in the case of early Martian missions. The dynamical boundary, where the magnetic field intensity has grown to 20–30 nT, and the fluxes of solar wind protons have decreased to the level of sensitivity of the sensors, was rediscovered. These characteristic features of the plasma and magnetic field behavior have again led the authors of papers [15–18] to the former concept that the magnetopause (MP) generated by the intrinsic dipole field similar to the MP of the Earth magnetosphere exists near Mars.

At the same time, according to the results of other plasma measurements on the same *Phobos-2* spacecraft, this boundary was called planetopause (PP) [19]. It was concluded that the PP does not always coincide with the pressure balance surface. The authors of [20] suggested that the PP was located significantly higher than the obstacle (the boundary of balance of pressures) predicted by the gas-dynamic model.

Analyzing jointly the data of the MAGMA magnetometer and the ASPERA plasma detector during the first three elliptical *Phobos-2* orbits, in paper [21], it was concluded that the PP represented the boundary in the chemical composition (the chemical boundary or the *ion composition boundary*), and that the PP may be an analogue of the upper ionospheric boundary, which has been observed on Venus during the periods of the high dynamic pressure of SW.

In 1997–1998, at the initial phase of revolution around Mars, the *Mars Global Surveyor* (*MGS*) spacecraft decelerated due to the friction in the atmosphere (*Aero Braking* or *AB* phase). The velocity of *MGS* near the pericenter decreased, and the spacecraft orbit changed from highly elliptical to nearly circular. The *AB* phase was divided into two subphases *AB1* and *AB2* with durations of 7 and 5 months, respectively, which

were separated by the phase of transfer into the science-oriented orbit (the *Science Phasing Orbit* or the *SPO* phase). The pericenter of the orbit during the AB phase descended to altitudes of 80–100 km. Due to the characteristics of the SC orbit, 80% of the data obtained during the *AB* phase were obtained on the dayside of Mars. On each of the orbits, the observations were used in the vicinity of the pericenter, i.e., approximately ±25° (north- and southward) from the point with latitude and longitude of the SC orbit pericenter because, with growing distance from the planetary surface, the intrinsic magnetic fields are weakening. The *AB1* and *AB2* subphases include a total of about 600 and 700 orbits, respectively. The altitudes of orbit pericenters and the other orbital parameters are presented on the website <http://mars.jpl.nasa.gov/mgs/status/nav/navhist.html>. During braking in the atmosphere, the latitude of the *MGS* orbit pericenter first gradually increased from 30° to 90°; then, for about 20 days, it sharply decreased to 0°. According to [22], the *MGS* magnetometer data were obtained in an altitude range of 80–450 km with nonuniform distribution in the areographical coordinates, and their accuracy was estimated to be approximately 3 nT.

The *MGS* discovered the localized magnetic anomalies on Mars [22]. The regions of intense magnetic anomalies on Mars (with the field up to 1600 nT at the altitude of 100 km) have large-scale structure and are thousands of kilometers extended along the longitude [23]. This indicates that, in the past, Mars possessed a magnetic dynamo. The remnant magnetic fields of Mars are concentrated mainly in the Southern Hemisphere of the planet, and only a few isolated groups of magnetic anomalies were observed in the Northern Hemisphere.

The lack of magnetic anomalies in the region of Hellas and Argon craters, which are believed to have been formed by impacts of asteroids 4 billion years ago, suggests that the dynamo effect, which is responsible for the crust magnetization, has stopped working before the moment when these impact craters have been formed.

The *MGS* did not have instruments for measuring the characteristics of ions, so it could not detect a boundary with the same characteristics of the PP as discovered on the *Phobos-2* SC. Meanwhile, the *MGS* observed a layer in which an increase in the magnetic field strength to 20–30 nT coexisted with decrease in the flux of energetic electrons (especially in the energy range of 20–200 eV) [24–26]. The wave activity in the magnetic field also decreased with decreasing altitude. The outer boundary of this layer was called the *magnetic pile–up boundary* (*MPB*). The extension of the *MPB* along the *MGS* trajectory ranged from several dozen to hundreds of kilometers.

Analyzing the *MGS* SC position at the entry or exit from the *MPB*, the authors of [24] obtained the average position of the *MPB* boundary and compared it with the average PP position obtained from the *Phobos-2* data. It was found that the PP, the boundary of ion composition or the chemical boundary, the boundary of the magnetic barrier, and the *MPB* are incarnations of the same phenomenon. The distinctions between the names of these boundaries found in the region of Mars' interactions with SWs are due to the fact that different experimental data or combinations of them were used to find them.

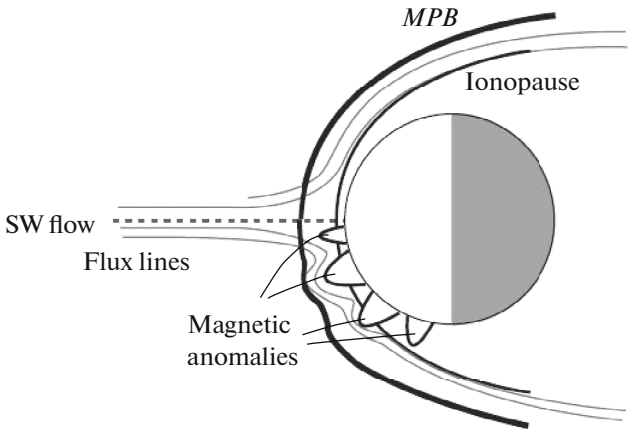

Fig. 1. It is schematically shown how the magnetic anomalies deflect the disturbed solar wind flowing around the Martian obstacle. In the Northern Hemisphere, except the only one large-scale magnetic anomaly, the flow around the upper boundary of the Martian ionosphere form the ionopause. In the Southern Hemisphere, the large-scale mini-magnetospheres, extending to altitudes higher than 400 km shift the closest to planet flow lines to higher altitudes.

According to [26, 27], the *MGS* data in the Southern Hemisphere as compared to those in the Northern Hemisphere clearly show the increase (on the average) in the MPB distance of moving from Mars (200 km) after its projection on the plane of the terminator (Fig. 1). Meanwhile, significant longitudinal variations of the *MPB* distance, projected on the terminator plane, were not detected, with the exception of increased variability in the longitude band of 90°–270°, where the remnant magnetic fields are the strongest.

Summarizing the measurements of the SW–Mars interactions based on the data of *Phobos-2* and *MGS* missions, one can state that the well-defined MPB boundary separates the region, which was called the *magnetic pile-up region* (*MPR*), from the magnetosheath (the region formed directly after the shock wave crossing by the SW flux) [28]. Despite that the SW proton and electron fluxes sharply drop at the *MPB* boundary, the IMF penetrates inside. Inside the *MPR*, on the dayside, the IMF increases and noticeably changes, drapping the planet. On the dayside the *MPR* is bounded from below by the upper boundary of the ionosphere, or by the exobase, depending on the solar wind pressure. Throughout almost the entire Northern Hemisphere of the planet and in the longi-

tude region from +120° to –120° (the Eastern longitude) of the Southern Hemisphere the SW directly interacts with the ionosphere and atmosphere of the planet.

The *MPB* and *MPR* have also been observed on Venus and comets, and they represent the general phenomenon of solar wind interaction with ionospheres and atmospheres of nonmagnetic or weakly magnetized bodies, which include Venus and, e.g., Halley's comet [29, 30].

On the nightside, the *MPR* is linked with the tail region that stretches for long distances behind the planet.

The plane of the circular *Phobos-2* orbit was located close to the Martian equatorial plane. In the magnetic tail of Mars the *Phobos-2* data were collected very closely to the equator, southward of which the remnant magnetic fields can balance the mean value of $p_{dyn} = 10^{-8}$ dyn/cm^2. Under these circumstances it is very difficult to distinguish the effects of longitudinal variations in remnant magnetic fields on the interactions with SWs in the Southern Hemisphere and the ionosphere effects on the interaction with SW in the Northern Hemisphere. We assume that a small value of change in the distance from the Martian surface to the PP at the terminator when changing p_{dyn} is due to the fact that, for $p_{dyn} > 10^{-8}$ dyn/cm^2, the combined effect of the local mode of the SW/remnant magnetic fields interactions in the Southern Hemisphere and the SW/ionosphere interaction in the Northern Hemisphere took place.

3. ANALYSIS OF THE MAGNETIC DATA

3.1. Distribution of magnetic flows associated with the residual magnetization of the crust. After performing experiments on *MGS*, it became evident that the magnetic fields near Mars represented a superposition of the induced component and remnant magnetic fields as follows:

$$\mathbf{B}(x, y, z) = \mathbf{B}_{\text{ind}}(x, y, z) + \mathbf{B}_{\text{crust}}(x, y, z).$$

Attempts to separate the induced field $\mathbf{B}_{\text{ind}}$ (x, y, z) and remnant magnetic fields $\mathbf{B}_{\text{crust}}(x, y, z)$ are based on the fact that $\mathbf{B}_{\text{crust}}(x, y, z)$ do not change during observations and are potential. A series of spherical harmonics is conventionally used to represent the potential fields, which only present the remnant magnetic fields outside the magnetized crust of Mars. The best approximation of the observed distribution of magnetic fields $\mathbf{B}(x, y, z)$ is selected using the least square technique. This approach is effective when the data almost uniformly cover all longitudes and latitudes and the measurements have rather high accuracy [31, 32]. The authors of [32] have shown that, in order for the calculations of Gaussian coefficients to be reliable up to a harmonic with a number of 44 (or even 30–35 at the conservative approach), for the uniform grid with a rectangular cell of 2° × 3°, the errors associated with the data that cover a spherical shell located at an altitude of about 400 km above the Martian surface should not exceed 2 nT. We note once again that, according to [22], the *MGS* magnetometer data were obtained in an altitude range of 80–450 km with a nonuniform distribution in geographical coordinates, and their accuracy was estimated to be about 3 nT. Then, according to [33], due to the various selections of data used to construct the approximation based on spherical harmonics, the constructed approximations turned out to be critically different when the number of the spherical harmonics exceeded 55–60. Spherical harmonics with numbers greater than 60 dominated at altitudes lower than 200 km. The measurements at altitudes lower than 200 km were only possible on the dayside of Mars during the *AB* phase. Because of this, the measurements at altitudes lower than 200 km had a high level of noises due to interactions with SW. The inclusion or exclusion of these noisy data determines the distinction between various approximations when the spherical harmonic number exceeds 55–60. Due to absence of an objective criterion for selecting experimental data and the rapid growth of noise with decreasing altitude, none of the existing models have an advantage. In the ionosphere region, all constructed approximations can either predict the phantom (nonexisting) anomalies or skip the strong remnant magnetic fields that actually exist.

The local but numerous magnetic anomalies that were discovered on the *MGS* can also generate the effective large-scale field. Despite the low values of the Gaussian coefficients in harmonics with a number lower than 5, these harmonics mainly determine the remnant magnetic field, when $\left(\frac{R_M}{R_M + h}\right)^{50} < 10^{-4}$–$10^{-3}$, ($R_M$ is the radius of Mars, h is the altitude), if the maximum of Gaussian coefficients is reached for $n = 50$–55, as in all works that were analyzed in [33].

The equivalent dipole method is widely used for representing the lithospheric magnetic fields on the Earth [34]. Initially, the equivalent dipole method was used in [35] in order that, using the radial component of magnetic fields measured on the *MGS* when passing low altitudes and previously redistributed in cells, to construct a map of the radial magnetic field component at the fixed altitude. Later, this model was revised in order to have the possibility of reproducing all three magnetic field components in the interval of altitudes of 173 km (the medium resolution of the model in the horizontal direction) to 430 km [31]. The magnetic data used in this model were obtained during the *AB1*, *SPO*, *AB2* and *MO* phases (1999) of the *MGS* mission. In the case of *AB* and *SPO* phases, only the measurements at altitudes lower than 350 km were used.

Thus, despite the evident progress in numerical modeling the remnant magnetic fields of Mars, the results of a qualitative analysis of magnetic fields mea-

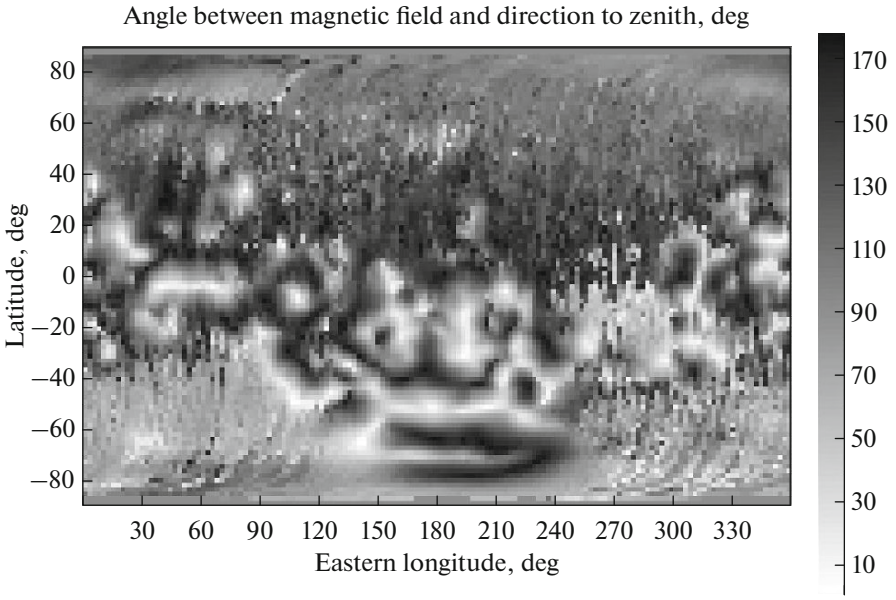

Fig. 2. Map of angles of Martian magnetic field with local zenith derived from *MGS* data.

sured at altitudes lower than 170–200 km remained very important.

Despite that the main part of the magnetic flow associated with the residual magnetization of the crust, it is concentrated near the Martian surface and the remaining magnetic flow moves away from the planet. This flow acts as an effective dipole, which occurs to be significantly stronger than the dipole component estimated in [36], 2×10^{17} A m^{-2}, which is associated exclusively with the processes occurring presently in the core.

It is seen from Fig. 2 that the effective magnetic flow sources, shown in white and light-grey color, are mainly concentrated in the Southern Hemisphere at latitudes lower than −20°. In addition, at latitudes lower than −20°, the majority of strong remnant magnetic fields are concentrated in the range of longitudes of 90°–250°, and these remnant magnetic fields apparently produce the main part of the radial magnetic flow of Mars.

For the numerical study of large-scale magnetic fluxes, one should use the radial magnetic field component measured on the nightside. This choice of data is an attempt to diminish the effect of the induced component and the compression of remnant magnetic fields at the interaction with SW [36].

During the measurements, the *MGS* has moved along the ellipsoidal surface with the focus at the Mars' center of masses. The analyzed data were obtained during 18 cycles of mapping in the period from March 1999 to August 2000, and then they were averaged. The averaging results were presented in the form of numerical maps of magnetic field components: B_r (in the radial planetocentric coordinate system), B_θ (in the south direction), and B_ϕ (in the east direction).

Because the *MGS* orbit did not change significantly during this period, i.e., the average for the time period T, the value of the flow through the element of the ellipsoidal surface Σ satisfies the relation

$$\begin{aligned}\langle\Phi\rangle &= \frac{1}{T}\int_0^T \Phi\,dt = \frac{1}{T}\int_0^T\left\{\int_\Sigma B_n d\Sigma\right\}dt \\ &= \int_\Sigma d\Sigma\left\{\frac{1}{T}\int_0^T B_n dt\right\} = \int_\Sigma d\Sigma\left(\mathbf{e}_n\cdot\frac{1}{T}\int_0^T \mathbf{B}\,dt\right) \\ &= \int_\Sigma d\Sigma(\mathbf{e}_n\cdot\langle\mathbf{B}\rangle),\end{aligned} \quad (1)$$

where B_n is the magnetic field component, which is directed along the external normal to the surface $\mathbf{e}_n$.

If the surface Σ is closed, then $\Phi = 0$, and the averaged magnetic field $\langle\mathbf{B}\rangle$ must satisfy the following relation:

$$\int_\Sigma d\Sigma(\mathbf{e}_n\cdot\langle\mathbf{B}\rangle) = 0. \quad (2)$$

In paper [37], this condition was verified by the numerical calculation of the expression $\Phi_{\text{eff}} \approx R_0^2(\pi/180)^2\sum_{i,j}(B_r)_{i,j}\sin(\pi/180\theta_i)$. This implies the following:

(1) The ellipsoid can be approximated by the sphere of radius $R_0 = R_M + 404$ km ($R_M = 3397$ km is the mean radius of Mars).

(2) The distinction between the direction of the external normal to the surface of ellipsoid $\mathbf{e}_n$ and the unit vector (ort) $\mathbf{e}_r$ of the planetocentric spherical coordinate system is negligible.

(3) $\langle \mathbf{B}_r \rangle$ is B_r of the numerical map of the magnetic field.

The first and second assumptions are fulfilled to an accuracy on the order of the ratio of the change in the *MGS* altitude (34 km) to the mean radius of its orbit of 3800 km, i.e., ≈1%. The third assumption requires more detailed discussion.

Magnetic measurements were carried out with fixed local Martian time. As already noted, $\mathbf{B}_{\text{crust}}(x, y, z)$ does not depend on time, and its contribution into Φ_{eff} should be close to zero. If Φ_{eff} occurs to be significantly different from zero, then this means that (a) the performed calibration has not completely eliminated the radial component of the field, which is generated by currents on the spacecraft itself and/or (b) essential asymmetry in the induced magnetic field associated with the Mars interaction with SW.

The full Φ_{eff} value for the whole Martian surface was calculated in [37] as 2.3×10^5 Tm^2 corresponds to the effective value $B_r = -1.6$ nT in each $1° \times 1°$ cell of the digital map and is close to the value of the undisturbed flow of IMF included in the spherical surface with radius equal to the radius of the Martian surface (the value of the undisturbed IMF near Mars equals 3–5 nT). It seems that the calculated value Φ_{eff} is too large for the induced magnetic field on the nightside of Mars because the majority of the IMF flow would have to be deflected by the ionosphere.

After excluding the systematic shift in the quantity $B_r = -1.6$ nT, in each $1 \times 1°$ cell of the digital map, for the region covering the latitudes lower than −20°, the calculated effective flow is $\Phi_{\text{res}} = 1.8 \times 10^5$ Tm^2. This is approximately equal to the flow generated by the dipole component of the magnetic field of Mars, estimated in paper [38].

At the same time, the flow from the sector located at a longitude of 90–250°, in which the strongest magnetic fields are concentrated, approximately equals $0.35\ \Phi_{\text{res}}$. Because this sector occupies about 44% of the total area of the region at latitudes lower than −20°, the region of strongest magnetic fields has a limited influence on the global structure of magnetic fluxes.

3.2. Mini-magnetospheres on the dayside of Mars. The closed field lines of extended linear structures with the opposite polarity in the Southern Hemisphere of Mars appear to form mini-magnetospheres [37], which are similar to the mini-magnetospheres first discovered on the lunar surface [39].

Since the plasma is a diamagnetic, it cannot penetrate into the regions of strong remnant magnetic fields from outside. As long as the field lines of remnant magnetic fields in this region remain closed, the region is isolated from both the rest ionosphere and SWs, and it can be considered as a closed mini-magnetosphere formed by remnant magnetic fields.

In order to determine the regions in which the measured fields represent mainly remnant magnetic fields using the map of magnetic fields measured at low altitudes of 170–180 km, the following criterion was used:

$$\frac{B^2}{8\pi} > \begin{cases} 2 \cdot 0.88 \cdot \cos^2\gamma \cdot 10^{-8}\ \text{dyn/cm}^2, & \gamma \le 70° \\ 2 \cdot 10^{-9}\ \text{dyn/cm}^2, & \gamma > 70°, \end{cases} \quad (3)$$

where γ corresponds to the latitude. The averaged dynamic SW pressure on the Martian orbit is equal to 10^{-8} dyn/cm^2. The distinctions in the Martian local time (MLT) during the field measurements and the increase of the altitude of the *MPR*/*MPB*, i.e., the region in which the SW flow deflection occurs, when moving from the subsolar point toward the terminator are ignored as long as $\gamma \le 70°$. For $\gamma > 70°$, the increase in the *MPB* altitude cannot yet be ignored. To take this fact into account, only the $\cos\gamma = \text{const}$ approximation was used. The multiplier 2 in the right-hand part of criterion (3) was introduced in order to ensure that, even at 12:00, when the SZA at the point of magnetic field measurements is minimum, the induced magnetic field could only accidentally satisfy criterion (3) in no more than 30% of all cases.

Figure 3 presents the characteristics of magnetic fields that do not satisfy criterion (3). Such fields can be expected to represent the IMF that envelops Mars.

Magnetic fields were measured at 170–180 km within the limits of three latitude intervals: 15°–30°, 30°–45° and 45°–60°. To compare these intervals, we normalized each calculated magnetic pressure by dividing it by $0.88 \cos^2\gamma$. Similarly to the diagrams for the normalized magnetic field pressure, for latitude intervals of 15°–30°, 30°–45°, and 45°–60°, the figure shows histograms of the angle between the magnetic field and the direction to the local zenith. As one can see, throughout the latitude range of 15°–60°, no considerable latitude dependence exists in either the distribution of angles or the normalized pressures.

Thus, if $\gamma \le 60°$, criterion (3) can efficiently distinguish the magnetic fields in the hemisphere of Mars that represent the IMF that envelops Mars.

The chosen latitude dependence in criterion (3) significantly lowers the regions on the map of magnetic fields in which a relatively strong induced field could be erroneously interpreted as remnant magnetic fields capable of forming a mini-magnetosphere near the terminator and on the nightside.

Figure 4 shows the map of pressure of magnetic fields measured at altitudes of 170–180 km on the dayside of Mars. Using criterion (3), the regions of predominant remnant magnetic fields were found. For the purposes of graphical representation in Fig. 4, it

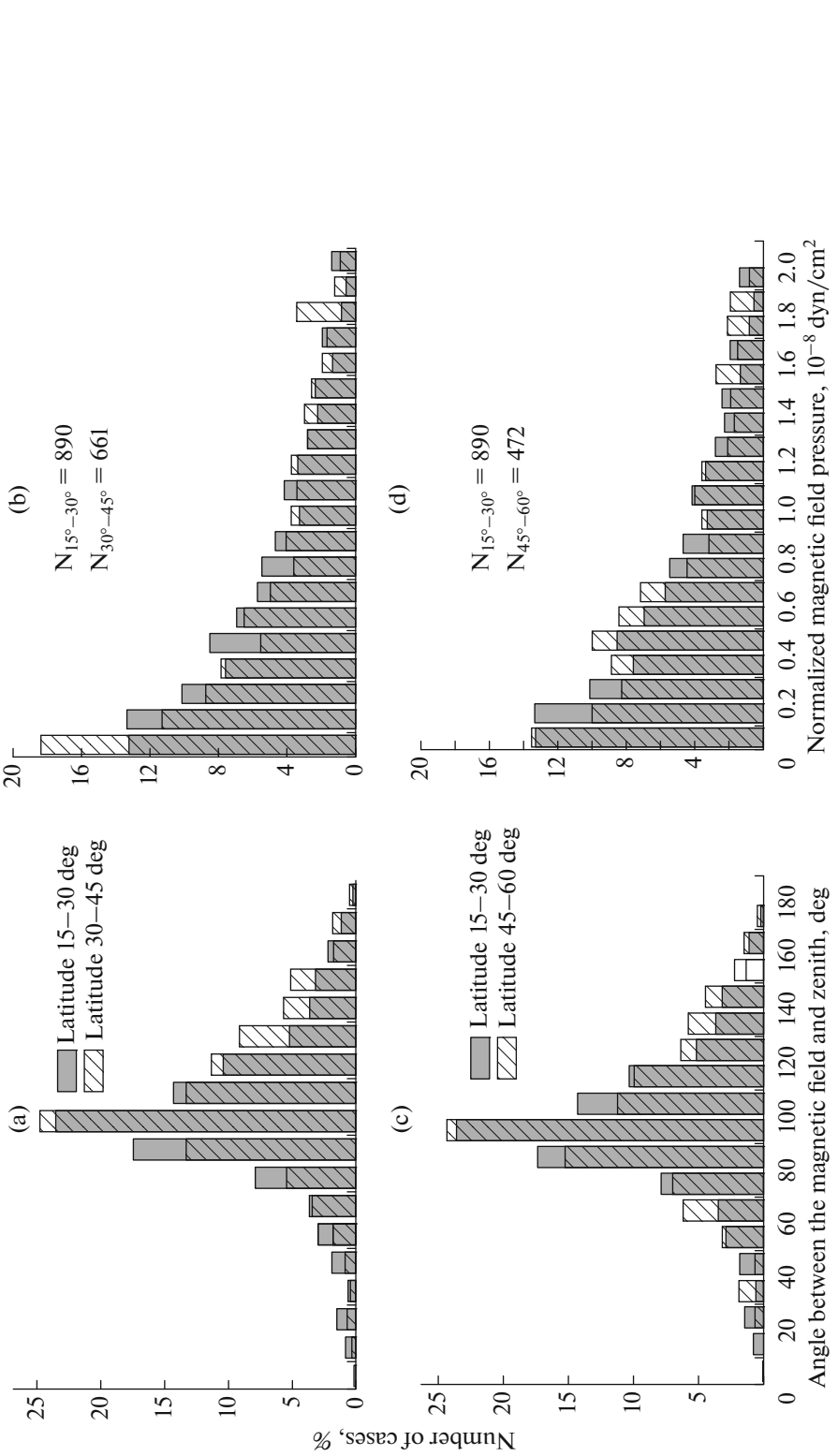

Fig. 3. Panels (a) and (c): histograms of the rate of occurrence of the angle between the local zenith and the magnetic field. Panels (b) and (d): histograms of the rate of occurrence of a normalized magnetic field pressure.

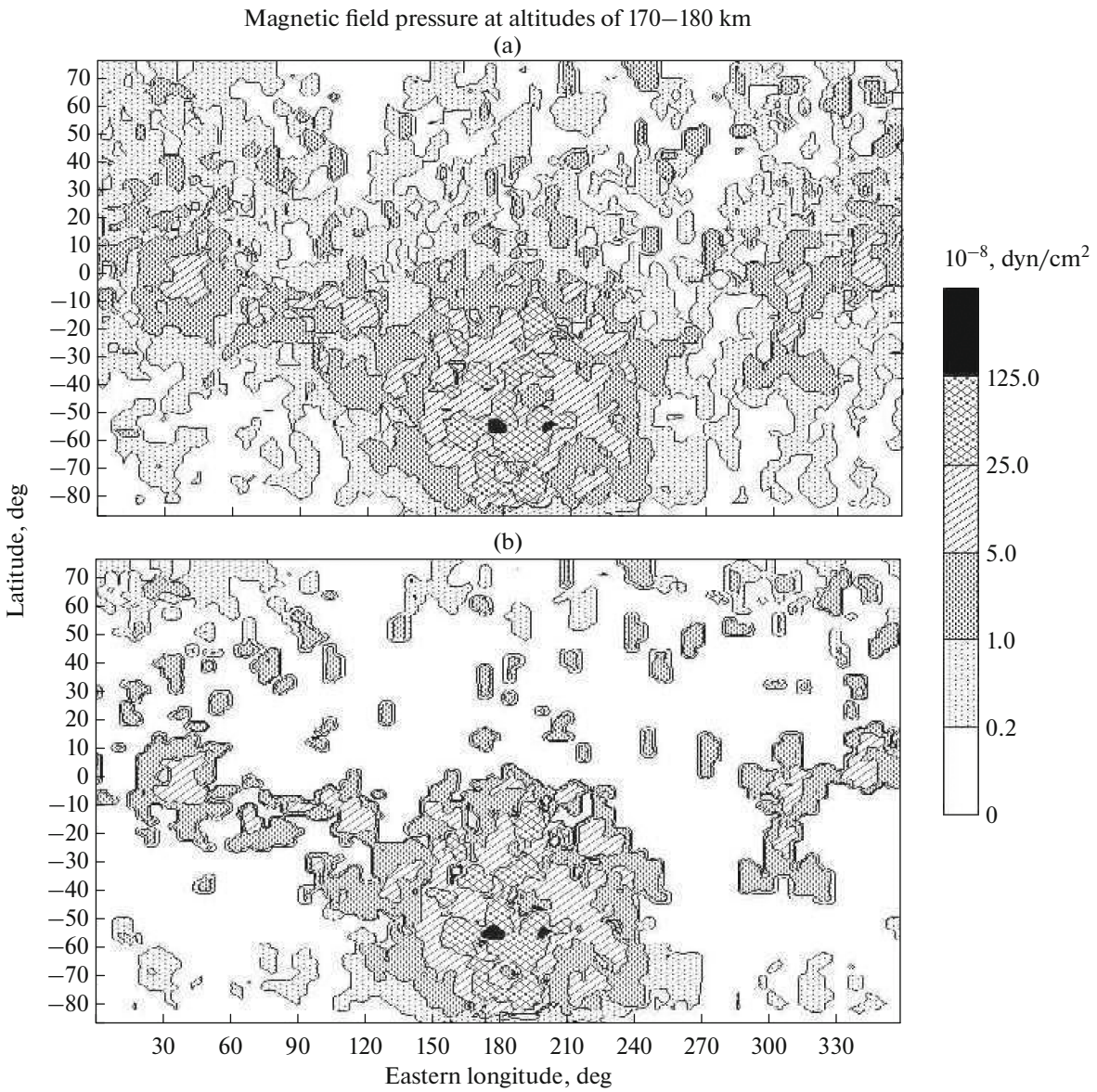

Fig. 4. Pressure of magnetic field measured at altitudes of 170–180 km.

was supposed that the pressure of magnetic fields, which do not satisfy criterion (3), is zero.

The mini-magnetospheres, determined from the data of measurements at altitudes of 170–180 km on the dayside of Mars, can also stretch to high altitudes on the nightside of Mars. The signs of such large mini-magnetospheres can be detected in the map of magnetic fields measured at altitudes of 400 km. The distinction between large and smaller mini-magnetospheres is that the magnetic field lines of force that are open after reconnection occupy a relatively large part of smaller mini-magnetospheres.

Comparing the pressure of magnetic fields measured at altitudes of 400 km with the Newtonian approximation of the pressure exerted on the mini-magnetosphere by the SW flow [40], one can determine the regions where the mini-magnetosphere can stretch to altitudes of 400 km and higher for the given value of the angle between the SW direction and the normal to the outer boundary of the potential mini-magnetosphere. The regions in which the pressure of magnetic fields exceeds the typical pressure exerted by the SW flow on the mini-magnetosphere when it is located near the terminator were determined under the assumption that the dynamic pressure of SW is equal to the average value of 10^{-8} dyn/cm^2, and the angle between the SW direction and the normal to the outer boundary of the potential mini-magnetosphere is constant and equal to 70°.

As can be seen in Fig. 5, in the Northern Hemisphere of Mars, the mini-magnetospheres usually are small in size and do not reach the altitudes of 400 km.

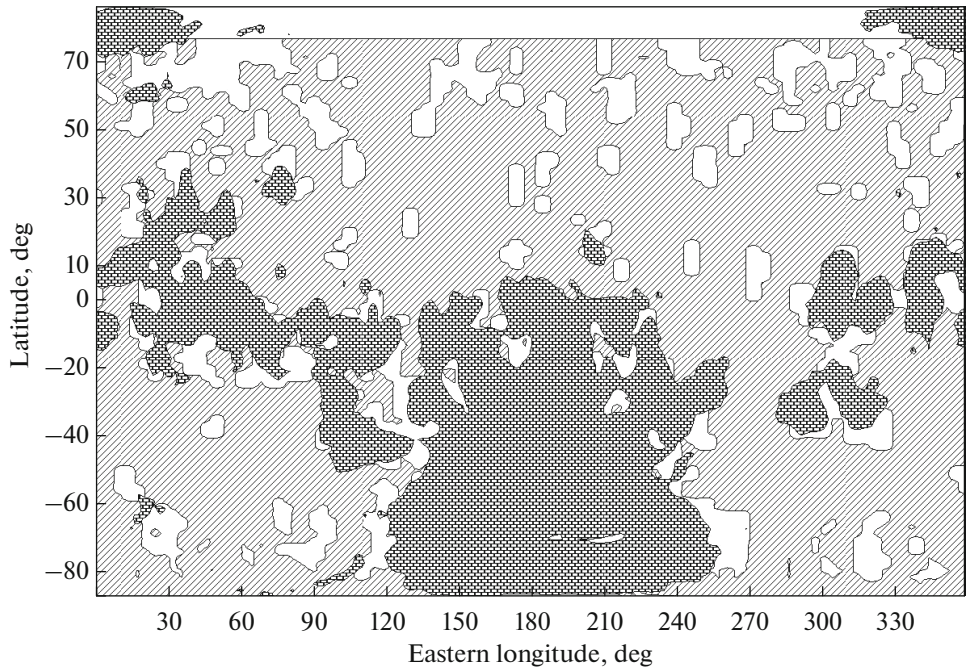

Fig. 5. Map of regions on Mars covered by large-scale and small-scale mini-magnetospheres. Large-scale mini-magnetospheres are indicated by brickwise hatching, small-scale mini-magnetosphere are indicated by white regions. Regions outside mini-magnetospheres are shaded.

In contrast, near the equator and in the Southern Hemisphere the larger-size mini-magnetospheres dominate.

3.3. Data collected in the tail of the Martian magnetosphere. Analyzing the places where the *Phobos-2* spacecraft intersects the boundary on which the SW proton fluxes fell below the sensitivity threshold of the TAUS instrument, the authors of [17] estimated the dipole moment of Mars as $(0.8–1.0) \times 10^{22}$ Gs cm^3 and supposed that the existing global magnetic field is strong enough to form the magnetospheric tail, the size of which, measured in radii of Mars, is significantly larger than the Venus magnetosphere size measured in radii of Venus [18]. At the same time, according to the estimate of the authors of paper [38], who have used the data of the *MAG/ER* experiment on the *MGS* SC, the dipole moment of Mars is about an order of magnitude smaller than the estimate in [18].

When analyzing the size of the magnetospheric tail, one should remember the following circumstances:

(a) At the outer boundary of the distant tail, $B_{\text{tail}}^2/8\pi = P_{\text{sw}}$, where B_{tail} is the strength of the magnetic field regardless of its nature and P_{sw} is the full pressure of SW flow on the orbit of Mars.

(b) The following relationship exists between B_{tail}, the full magnetic flow in the lobe of the tail ϕ (regardless of its nature) and the cross-sectional area of the tail $-\Sigma$: $B_{\text{tail}} \approx \phi/\Sigma$. Thus, the larger the value of ϕ (regardless of its nature), the greater the size of the tail.

It is obvious that, in the presence of remnant magnetic fields, the intrinsic magnetic dipole moment of Mars will be overestimated, if one attributes the whole magnetic flow ϕ (regardless of its nature) solely to the magnetic dipole associated with the processes in the core of the planet.

3.4. Cusps and reconnection of remnant magnetic fields with the IMF. After the reconnection of the remnant magnetic fields with the IMF enveloping the mini-magnetosphere, the external boundary of the closed mini-magnetosphere becomes adjacent to the boundary layer with the open field lines that connect the SW and the surface of Mars. Some part of energetic SW protons and electrons propagating along the open lines of force are reflected backward from the regions of enhanced magnetic field, but the magnetic field has a small effect on the propagation of the main part of SW protons and electrons. In the reconnection region, the main part of SW protons and electrons can penetrate into the dense layers of the atmosphere (up to the exobase and even below).

The bases of the external lines of force of remnant magnetic fields (the Martian surface intersection by the field lines) are located in the regions of cusps. For the altitude interval of 80–200 km (measurements on the dayside of Mars), in the Southern Hemisphere in 10–15% of all cases, the angle with the direction to zenith is either <30°, or >150° (see Fig. 3 in [37]). This allows SW particles to penetrate into the lower atmosphere after reconnection. The authors of [41] have studied the reconnection of Martian remnant mag-

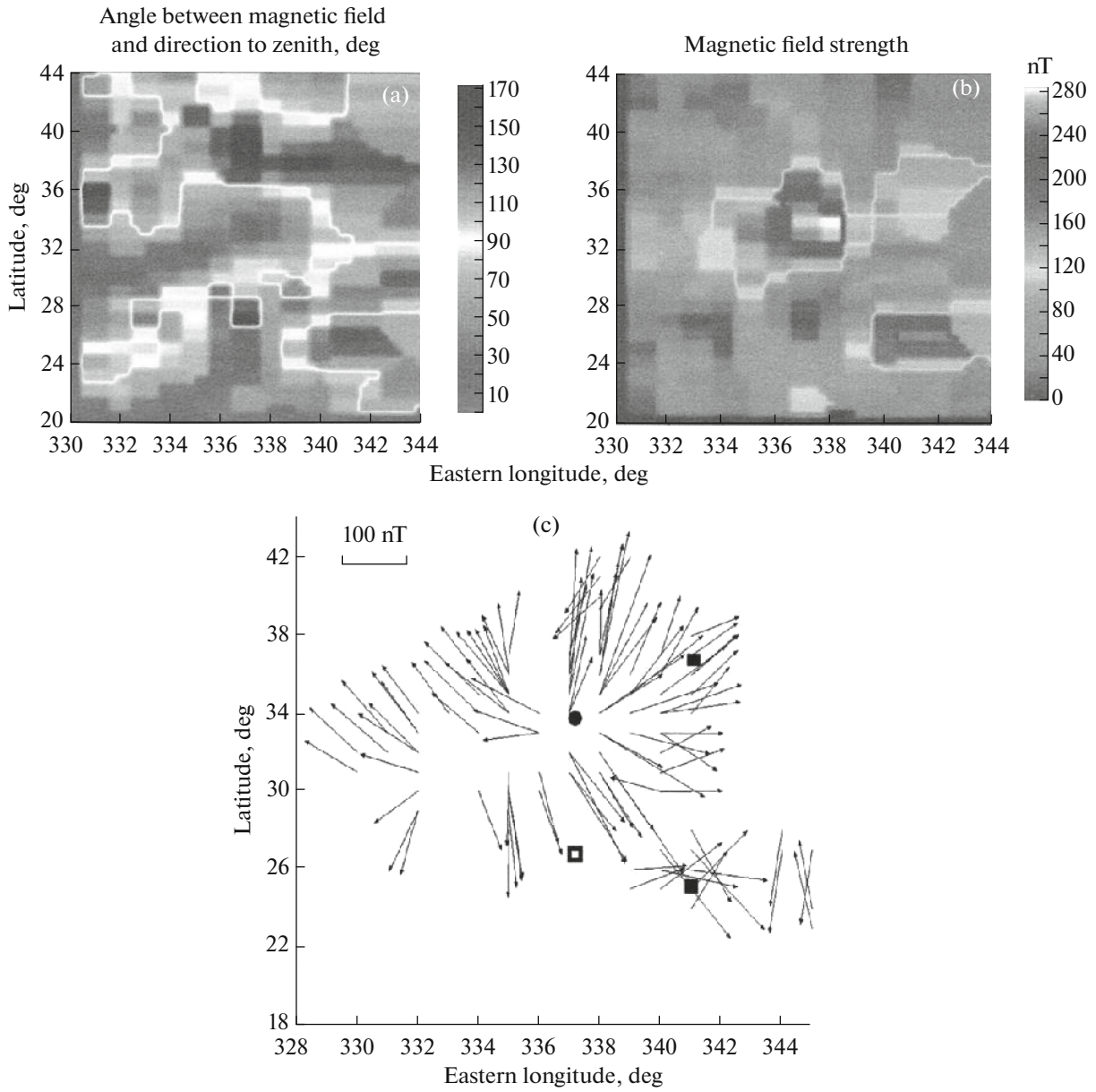

Fig. 6. Angle between the magnetic field and the direction to zenith, deg.

netic fields with IMF and found that the reconnection regions can capture about 7% of the surface of Mars.

In the reconnection process, the open field lines of remnant magnetic fields determine the direction of fluxes of energetic particles of SW, so that their precipitation occurs in the vicinity of magnetoconjugate points. It is obvious that the remnant magnetic fields should determine the position of magnetically conjugate points. To illustrate this statement, Figure 6 presents maps of the angle with the direction to zenith in the (a) vicinity and (b) magnetic field strength of the isolated magnetic anomaly with aerocentric coordinates 34° N, 337° E, and on the panel the c—map of the horizontal magnetic field component is shown. To reduce the effect of the induced component of the magnetic field, the map shows only the horizontal component that exceeds the threshold of 100 nT. It appears that, in the region of the anomaly, there are three localized sources of remnant magnetic fields with coordinates, i.e., 34° N, 337° E; 25° N, 341° E; and 37° N, 341° E. The weak field region around the point of 27° N, 337° E is obviously magnetically conjugate one with the strong field in the region of 34° N, 337° E. Thus, if the reconnection occurs at the point of 34° N, 337° E, the precipitation of SW particles can be observed near the point of 27° N, 337° E, i.e., at a distance of 400–500 km from the precipitation point.

The SPICAM experiment onboard the *Mars Express* spacecraft recorded the local glow of the atmosphere, which was much more intensive than that on Venus

[42]. This glow, i.e., the aurora, is caused by the highly localized precipitation of electrons into the Martian atmosphere. The position of the observed glow correlates with the position of magnetic anomalies discovered on the *MGS*. This turned out to be a direct experimental confirmation of the association of precipitations of energetic SW electrons with the reconnection of magnetic field lines.

In the experiments with the analyzer of plasma and energetic atoms on the *Mars Express* spacecraft [43], the researchers performed a detailed study of the acceleration processes in the deep region of the nightside of Mars, which geographically coincided with the region of the localization of magnetic anomalies. Integrating the energy of electrons and ions, the flows of which were directed upward and downward in the upper atmosphere, the authors obtained the energy of the order of 1–50 mW $m^{-2}s^{-1}$. This energy flow produces bright discrete auroras on the Earth. The map of distribution of magnetic force tubes is constructed in which the precipitation can occur, and it lies in the regions of cusps of magnetic anomalies (see Fig. 4 in [43]).

3.5. Retention of a weak remnant magnetic field below the maximum thermal pressure of plasma. The event of the retention of the horizontal magnetic field in the lower ionosphere of the planet was initially analyzed in an unpublished report by Johnston and Axford [10]. Below the thermal pressure maximum, both the gravity force and the thermal pressure gradient are acting in the same direction, and the force $[\mathbf{j}\times\mathbf{B}]$ helps the force of friction over the neutral atmosphere balance them.

Table 1 presents the rate of appearance (in per cents) of strong magnetic fields of the crust that which do not satisfy criterion (3) for the latitude interval of 15°–30° and the total number of magnetic field measurements in five altitude intervals, i.e., 170–180, 150–160, 130–140, 110–120, and 90–100 km. The increase in the percentage of strong crustal magnetic fields from 9% at 170–180 km up to 28% at 110–120 km indicates the greater effect of crust magnetization at low altitudes. The lower percentage of strong magnetic fields of the crust at 90–100 km than at 110–120 km may be a consequence of the relatively small number of magnetic field measurements at altitudes of 90–100 km.

Table 1. Statistical indicators of strong crustal magnetic fields that do not satisfy criterion (3) for a latitude interval of 15°–30°

Altitude interval, km	Total number of magnetic field measurements	Percentage of strong fields of the crust
170–180	981	9
150–160	940	14
130–140	966	23
110–120	1517	28
90–100	141	23

4. FORMATION OF SMALL-SCALE STRUCTURES IN THE MAGNETIC FIELD

As previously on Venus, the small-scale flax ropes of the magnetic field were observed on Mars [44]. However, according to [45], these ropes were observed rather rarely, i.e., in 5% of all cases of elliptical *MGS* orbits. Small-scale flax ropes of the magnetic field have not been detected in the Southern Hemisphere of Mars and, in the Northern Hemisphere, they have been recorded near the terminator at altitudes lower than 400 km. These magnetic flux ropes were randomly oriented in space, whereas on Venus they were predominantly horizontal [45].

After discovering the magnetic flux ropes on Venus, it was supposed that they arose as a result of development of the Kelvin–Helmholtz instability, which was caused by the altitudinal gradient of the horizontal velocity of a plasma flow [44, 46]. The increment of this instability is sensitive to the flow velocity orientation relative to the magnetic field in plasma such that the Kelvin–Helmholtz instability does not develop in the subsolar region of Venus due to the relatively low velocities and enhanced magnetic field in the transition region [47].

In paper [14], it was shown that the upper part of the magnetic belt formed in the Venusian ionosphere, where $dB/dz < 0$, is unstable. The destruction of the magnetic belt may explain the fact that, on Venus, during some periods, the small-scale flux ropes were observed slightly above the region of the magnetic belt filled with a large-scale magnetic field. However, on Mars no signs of the formation of a magnetic belt were found [48]; thus, the mechanism that works on Venus is ineffective on Mars.

Finally, in paper [49], it was hypothesized that, on Venus, the magnetic flux ropes can be formed under the action of internal gravity waves. However, the author of [50] pointed out that the proposed mechanism is only valid if the rate of ion collisions with neutrals is higher than the gyro frequency of ions in the large-scale magnetic field in the ionosphere. On Mars, where the atmosphere is rarefied and the magnetic fields in the ionosphere are relatively strong, under normal conditions, the internal gravity waves are unlikely to form small-scale magnetic flux ropes.

All of this may explain the fact that, on Mars, unlike Venus, small-scale flax ropes of the magnetic field are observed rather rarely.

CONCLUSIONS

1. The remnant magnetization of the crust on Mars leads to the situation where the planetary magnetic fields were observed both in the ionosphere region and

above it (at altitudes of 400 km on the nightside of Mars).

2. The outmost field lines of remnant magnetic fields that form mini-magnetospheres can be reconnected with the IMF. The feet of those magnetic field lines (i.e., the places where they meet the surface of Mars) indicate the regions in which the precipitation of energetic particles takes place after reconnection.

3. In the regions of numerous cusps of mini-magnetospheres, the precipitating energetic particles penetrate deep into the atmosphere/thermosphere and cause the heating and expansion of the atmosphere/thermosphere. The energetic electrons may cause additional ionization by electron impact and glow of the atmosphere.

4. After reconnection, the energetic particles precipitate at magnetically conjugate points. As a result, the precipitating particles can heat the atmosphere not only in the area of cusps, but in halo regions, which are located hundreds of kilometers from the cusps. The remnant magnetic anomalies near 34° N and 337° E (see [53]) represent a perfect example of this situation.

5. The horizontal magnetic fields (associated both with magnetic anomalies and IMF drapped around Mars) determine the features of plasma distribution in the Martian ionosphere observed in radio occultation experiments that differ from the situation on the other nonmagnetized planet, i.e., Venus. In particular, (a) the approximate constancy of the scale heights of electron density in the ionosphere and (b) the absence of the flaring of the Martian ionosphere's upper boundary (an insignificant or zero increase in its altitude from the subsolar region toward the terminator).

REFERENCES

1. Connerney, J.E.P., Espley, J., Lawton, P., et al., The MAVEN magnetic field investigation, *Space Sci. Rev.*, 2015, vol. 195, no. 1, pp. 257–291. doi 10.1007/s11214-015-0169-4
2. Dolginov, Sh., Yeroshenko, Ye.G., and Zhuzgov, D.N., Magnetic field of Mars according to data Mars-3 and Mars-5 satellites, *J. Geophys. Res.*, 1976, vol. 81, pp. 3353–3362.
3. Dolginov, Sh.Sh., Yeroshenko, Ye.G., Zhuzgov, L.N., et al., Magnetic field and plasma inside and outside of the Martian magnetosphere, in *Solar Wind Interaction with the Planets Mercury, Venus and Mars* (NASA, Washington, D.C., 1976), pp. 1–20.
4. Gringauz, K.I., Interaction of solar wind with Mars as seen by charged particle traps on Mars 2, 3 and 5 satellites, *Rev. Geophys. Space Phys.*, 1976, vol. 14, no. 3, pp. 391–402.
5. Breus, T.K. and Verigin, M.I., Study of solar plasma near Mars and on the Earth–Mars route using charged particle catchers on Soviet space vehicles in 1971–1973, *Kosm. Issled.*, 1976, vol. 14, no. 3, pp. 400–405.
6. Bogdanov, A.V. and Vaisberg, O.L., Structure and variations of the solar wind–Mars interaction region, *J. Geophys. Res.*, 1975, vol. 80, pp. 487–494.
7. Dolginov, Sh.Sh., On the magnetic field of Mars: Mars 2 and 3 evidence, *Geophys. Res. Lett.*, 1978, vol. 5, no. 1, pp. 89–92.
8. Sibeck, D.G., Lopez, R.E., and Roelof, E.C., Solar wind control of the magnetopause shape, location and motion, *J. Geophys. Res.*, 1991, vol. 96, pp. 5489–5495.
9. Russell, C.T. and Vaisberg, O., The interaction of the solar wind with Venus, in *Venus*, Hunten, D.M., , Ed., Tucson: Univ. of Arizona, 1983, pp. 873–940.
10. Krymskii, A.M., An interpretation of the large-scale ionospheric magnetic fields and the altitude distribution of the ionospheric plasma on the dayside of the Venus and Mars, in *Venus and Mars: Atmosphere, Ionospheres and Solar Wind Interactions*, Luhmann, J.G., Tatrallyay, T., and Pepin, R.O., Eds., Washington, D.C.: AGU, 1992.
11. Hanson, W.B. and Mantas, G.P., Viking electron temperature measurements–evidence for a magnetic field in the Martian ionosphere, *J. Geophys. Res.*, 1988, vol. 93, no. 1, pp. 7538–7544.
12. Breus, T.K., Bauer, S.J., Krymskii, A.M., and Mitnitskii, V.Ya., Mass-loading in the solar wind interaction with Venus and Mars, *J. Geophys. Res.*, 1989, vol. 94, pp. 2375–2382.
13. Brecht, S.H. and Ferrante, J.R., Global hybrid simulation of unmagnetized planets: Comparison of Venus and Mars, *J. Geophys. Res.*, 1991, vol. 96, pp. 11209–11220.
14. Krymskii, A.M., Breus, T.K., Ness, N.F., and Acuna, M.H., The IMF pile-up regions near the Earth and Venus: Lessons for the solar wind–Mars interaction, *Space Sci. Rev.*, 2000, vol. 92, pp. 535–564.
15. Rosenbauer, H., Shutte, N., Apathy, I., et al., Ions of Martian origin and plasma sheet in the Martian magnetosphere: Initial results of the TAUS experiment, *Nature*, 1989, vol. 341, pp. 612–614.
16. Lundin, R., Zakharov, A., and Pellinen, R., First measurements of the ionospheric plasma escape from Mars, *Nature*, 1989, vol. 341, pp. 609–612.
17. Verigin, M.I., Gringauz, K.I., Kotova, G.A., et al., The dependence of the Martian magnetosphere and bow shock on solar wind ram pressure according the Phobos-2 TAUS ion spectrometer measurements, *J. Geophys. Res.*, 1993, vol. 98, pp. 1303–1309.
18. Verigin, M., Kotova, G., Shutte, N., et al., Quantitative model of the Martian magnetopause shape and its variation with the solar wind Ram pressure based on Phobos-2 observations, *J. Geophys. Res.*, 1997, vol. 102, no. 2, pp. 2147–2155.
19. Trotignon, J.G., Grard, R., Barabash, S., et al., Solar wind measurements near Mars and their implication in the red planet environment, *Planet. Space Sci.*, 1996, vol. 44, no. 2, pp. 117–127.
20. Grard, R., Skalsky, S., and Trotignon, J.G., Selected wave and plasma features of the Martian environment, in *Plasma Environments of Non-Magnetic Planets, (COSPAR Colloquia Ser. 4)*, New York: Pergamon, 1993, p. 321.
21. Breus, T.K., Dubinin, E.M., Krymskii, A.M., et al., The solar wind interaction with Mars: Consideration of Phobos 2 mission observations of an ion composition

boundary on the dayside, *J. Geophys. Res.*, 1991, vol. 96, pp. 11165–11174.

22. Acuna, M.H., Connerney, J.E.P., Wasilewski, P., et al., Magnetic field and plasma observations at Mars: Initial results of the Mars Global Surveyor mission, *Science*, 1998, vol. 279, pp. 1676–1680.
23. Connerney, J.E.P., Acuna, M.H., Wasilewski, P.J., et al., The global magnetic field of Mars and implications for crustal evolution, *Geophys. Res. Lett.*, 2001, vol. 28, pp. 4015–4018.
24. Vignes, D., Mazelle, C., Rueme, H., et al., The solar wind interaction with Mars: Locations and shapes of the bow shock and the magnetic pile-up boundary from the observations of the MAG/ER experiment onboard Mars Global Surveyor, *Geophys. Res. Lett.*, 2000, vol. 27, no. 1, pp. 49–52.
25. Cloutier, P.A., Law, C.C., Crider, D.H., et al., Venus-like interaction of the solar wind with Mars, *Geophys. Res. Lett.*, 1999, vol. 26, no. 17, pp. 2685–2688.
26. Crider, D.H., Cloutier, P., Law, C., et al., Evidence of electron impact ionization in the magnetic pileup boundary of Mars, *Geophys. Res. Lett.*, 2000, vol. 27, no. 1, pp. 45–48.
27. Crider, D.H., Acuña, M.H., Connerney, J.E.P., et al., Observations of the latitude dependence of the location of the Martian magnetic pileup boundary, *Geophys. Res. Lett.*, 2002, vol. 29, no. 8, pp. 11-1–11-4.
28. Nagy, A.F., Winterholter, D., Sauer, K., et al., The plasma environment of Mars, *Space Sci. Rev.*, vol. 111, nos. 1–2, pp. 33–114. doi 10.1023/B:SPAC.0000032718.47512.92
29. Breus, T.K., Venus: Review of present understanding of solar wind interaction, *Space Sci. Rev.*, 1979, vol. 23, pp. 253–275.
30. Verigin, M.I., Gringauz K.I., Rishter A.K. et al., Plasma properties from the upstream region to the cometopause of comet Halley: Vega observations, *Astron. Astrophys*, 1987, vol. 187, pp. 121–124.
31. Langlais, B., Purucker, M.E., and Mandea, M., Crustal magnetic field of Mars, *J. Geophys. Res.*, 2004, vol. 109, E02008. doi 10.1029/2003JE002048
32. Schmitz, D.R., Meyer, J., and Cain, J.C., Modelling the Earth's geomagnetic field to high degree and order, *Geophys. J.*, 1989, vol. 97, pp. 421–430.
33. Arkani-Hamed, J., A 50-degree spherical harmonic model of the magnetic field of Mars, *J. Geophys. Res.*, 2001, vol. 106, pp. 23197–23208.
34. Langel, R.A. and Hinze, W.J., *The Magnetic Field of the Earth's Lithosphere: The Satellite Perspective*, New York: Cambridge Univ. Press, 1998.
35. Purucker, M., Ravat, D., Frey, H., et al., An altitude normalized magnetic map of Mars and its interpretation, *Geophys. Res. Lett.*, 2000, vol. 27, pp. 2449–2452.
36. Acuña, M.H., Connerney, J.E.P., Wasilewski, P., et al., Magnetic field of Mars: Summary of results from the aerobraking and mapping orbits, J. Geophys. Res., 2001, vol. 106, pp. 23403–23417.
37. Krymskii, A.M., Breus, T.K., Ness, N.F., et al., Structure of the magnetic field fluxes connected with crustal magnetization and topside ionosphere at Mars, *J. Geophys. Res.*, 2002, vol. 107, no. A9, pp. SIA 2-1–SIA 2-10.
38. Cain, J.C., Ferguson, B.B., and Mozzoni, D., An $n = 90$ internal potential function of the Martian crustal magnetic field, *J. Geophys. Res.*, 2003, vol. 108, no. E2. doi 10.1029/2000JE001487
39. Lin, R.P., Mitchell, D.L., Curtis, D.W., et al., Lunar surface magnetic fields and their interaction with the solar wind: Results from lunar prospector, *Science*, 1998, vol. 281, pp. 1480–1484.
40. Spreiter, J.R. and Stahara, S.S., Computer modeling of the solar wind interaction with Venus and Mars, in *Venus and Mars: Atmosphere, Ionospheres, and Solar Wind Interactions*, Luhmann, J.G., Tatrallyay, M., Pepin, R.O., Eds., Washington, D.C.: AGU, 1992, pp. 345–383.
41. Brain, D.A., Bagenal, F., Acuña, M.H., and Connerney, J.E.P., Martian magnetic morphology: Contributions from the solar wind and crust, *J. Geophys. Res.*, 2003, vol. 108, no. A12, 1424. doi 10.1029/2002JA009482
42. Bertaux, J.-L., Leblanc, F., Perrier, S., et al., Nightglow in the upper atmosphere of Mars and implications for atmospheric transport, *Science*, 2005, vol. 307, pp. 566–569.
43. Lundin, R., Winningham, D., Barabash, S., et al., Plasma acceleration above Martian magnetic anomalies, *Science*, 2006, vol. 311, pp. 980–983.
44. Cloutier, P.A., Tascione, T.F., Daniell, E., et al., Physics of the interaction of the solar wind with the ionosphere of Venus: Flow/field models, in *Venus*, Hunten, D.M., , Ed., Tucson: Univ. of Arizona, 1983, pp. 941–979.
45. Vignes, D., Acuña, M.H., Connerney, J.E.P., et al., Magnetic flux ropes in the Martian atmosphere: Global characteristics, in *Mars' Magnetism and its Interaction with the Solar Wind*, Winterhalter, D., Acuña, M., and Zakharov, A., Eds., Dordrecht: Springer, 2004, pp. 223–231.
46. Wolff, R.S., Goldstein, B.E., and Yeates, C.M., The onset and development of Kelvin–Helmholtz instability at the Venus ionopause, *J. Geophys. Res.*, 1980, vol. 85, no. A13, pp. 7697–7707.
47. Krymskii, A.M., On the stability of Venus' ionopause, *Kosm. Issled.*, 1987, vol. 25, no. 3, pp. 456–463.
48. Kireev, A.P. and Krymskii, A.M., Neutral atmosphere and crustal magnetization as factors determining differences in plasma convection and magnetic fields distribution in the ionospheres of Mars and Venus, *Adv. Space Res.*, 2012, vol. 49, no. 3, pp. 458–466. doi 10.1016/j.asr.2011.09.025
49. Luhmann, J.G. and Elphic, R.C., On the dynamo generation of flux ropes in the Venus ionosphere, *J. Geophys. Res.*, 1985, vol. 90, pp. 12047–12056.
50. Cole, K.D., Origin of flux ropes in Venus' ionosphere, *J. Geophys. Res.*, 1994, vol. 99, no. A8, pp. 14951–14958.

Translated by Yu. Preobrazhensky